Supporting Material

Harnessing Anisotropy in Liquid Crystal Elastomer based Lithium-ion Gel-Polymer Batteries

Zakaria Siddiquee [1], Weinan Xu [2], Antal Jákli [3,*]

[1] Department of Physics, Kent State University, Kent, OH 44242, USA
[2] School of Polymer Science and Polymer Engineering, University of Akron, Akron, Ohio 44325, USA
[3] Materials Science Graduate Program and Advanced Materials and Liquid Crystal Institute, Kent, OH 44242, USA

This material composition for LCE-Xn, where X = P (Planar) or H (Homeotropic), is listed in **Table S1**.

Table S1: Material composition of electrolytes. * The catalyst solution is prepared by dissolving a specified weight percentage (wt.%) of DPA in toluene.

	RM257 (mg)	**BMIM-TFSI** (mg)	**LiTFSI** (mg)	**EDDET** (mg)	**PETMP** (mg)	**BHT** (mg)	**IRG651** (mg)	**DPA** (mg)
LCE-X1	500	5	100	105.7	47.1	1.33	3.77	78.4 (2 wt.%)*
LCE-X2	500	250	100	105.7	47.1	1.33	3.77	78.4 (2 wt.%)*
LCE-X3	500	500	100	105.7	47.1	1.33	3.77	78.4 (2 wt.%)*
LCE-X4	500	1000	100	105.7	47.1	1.33	3.77	78.4 (2 wt.%)*
LCE-X5	500	1500	100	105.7	47.1	1.33	3.77	78.4 (0.5 wt.%)*

In **Figure S1(a)**, the FTIR spectra of the individual components of the elastomer are shown, with the relevant peaks corresponding to S–H, C=C, and C=O highlighted. The elastomer is formed in two sequential stages. In the first stage, a Michael addition reaction occurs, in which thiols act as versatile functional groups capable of reacting with various other functionalities to form polymeric products. Specifically, thiols react with (meth)acrylates.[1,2] This reaction is evidenced in the FTIR spectrum by a peak at 2507 cm^{-1}, indicative of the thiol–methacrylate linkage.

In the second stage, activation of the photoinitiator via UV irradiation triggers the ene–ene reaction of RM257 functional groups, resulting in the formation of a crosslinked polymer network. The C=C stretching vibration associated with this crosslinking is observed at 1606 cm^{-1}. **Figures S1(b)** and **S1(c)** show these features for elastomers with planar and homeotropic alignments respectively, demonstrating the influence of molecular orientation on the FTIR response of the cured elastomer.

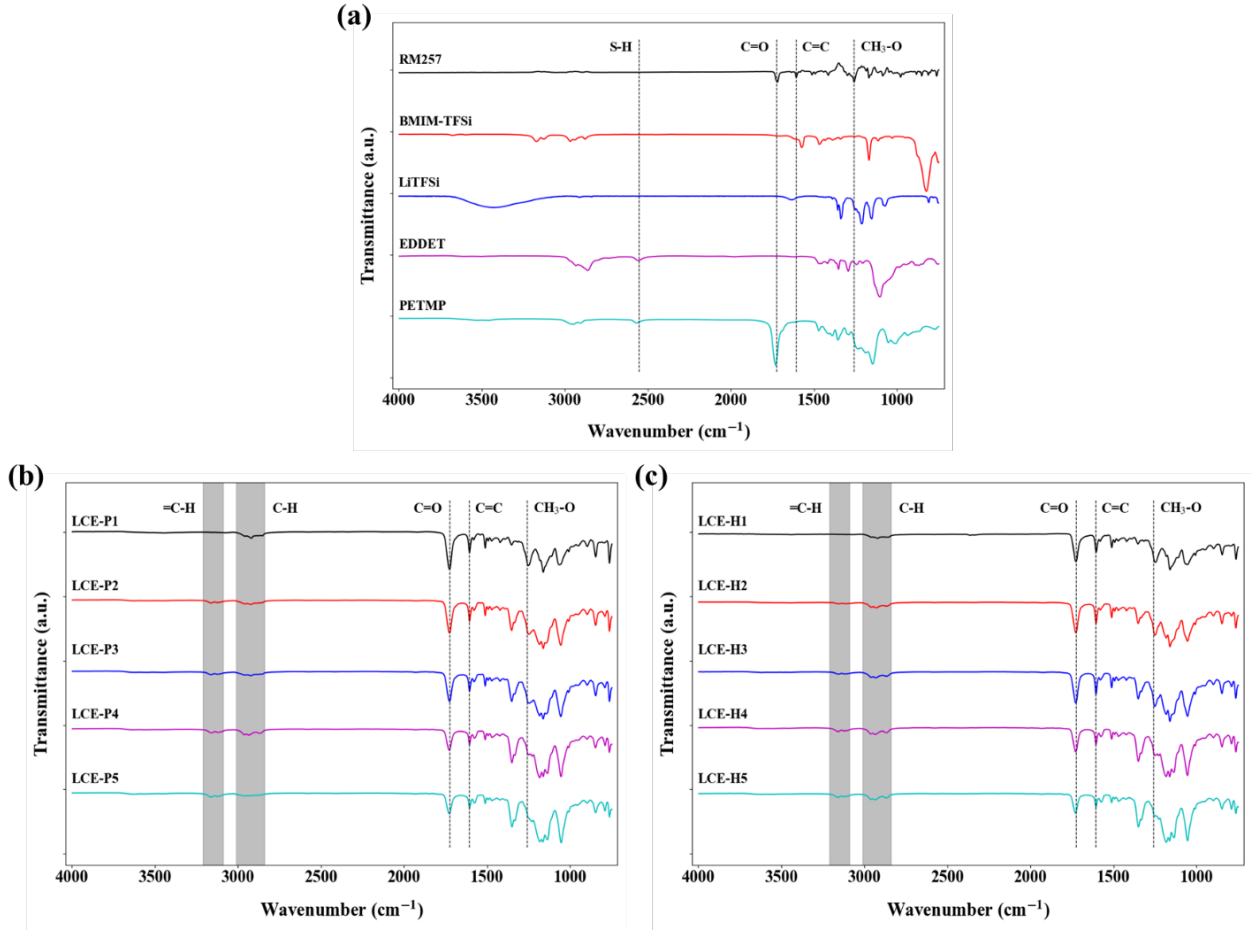

Figure S1: FTIR spectra of precursor materials and aligned elastomer electrolytes. (a) FTIR spectra of RM257 monomer, chain extender EEDET, crosslinker PETMP, ionic liquid BMIM-TFSI, and lithium salt LiTFSI. FTIR spectra of the LCE-Xn series of electrolytes, with relevant bond signature wavelengths indicated. (b) Planar-aligned and (c) homeotropic-aligned electrolytes.

1D Wide Angle X-Ray Scattering (WAXS) 2D intensity vs q data with corresponding spectra with 300s exposure time for the planar and homeotropic LCE-Xn (n = 2, 3, 4, 5) samples are presented in **Figures S2** and **Figures S3**, respectively. For the planar samples, the elastomers were placed flat on the sample holder with 3 mm diameter holes, ensuring that the director was oriented vertically. The diffraction patterns along the horizontal axis gradually weaken from **Figure S3(a)** to **S3(d)**, indicating that the X-ray beam is increasingly disturbed as the ionic liquid content rises or the degree of alignment decreases. In **Figure S3(d)**, the appearance of a ring pattern suggests that the sample is unaligned, with alignment effects largely minimized.

For homeotropic samples, initial spectra were recorded with the director pointing into the plane of the page; however, only a diffuse ring was observed, providing no additional structural information. As shown in **Figure S3(e-h)**, the samples were oriented such that the director also faced vertically. To achieve this, the elastomers were cut along their diameter to a thickness of 100 μm and mounted on a sample holder with 0.5 mm diameter holes. The resulting diffraction patterns exhibit trends like those observed in the planar samples. From **Figure S3(e)** to **S3(h)**, the intensity of the diffraction gradually decreases, reflecting a reduction in the degree of alignment with increasing ionic liquid content.

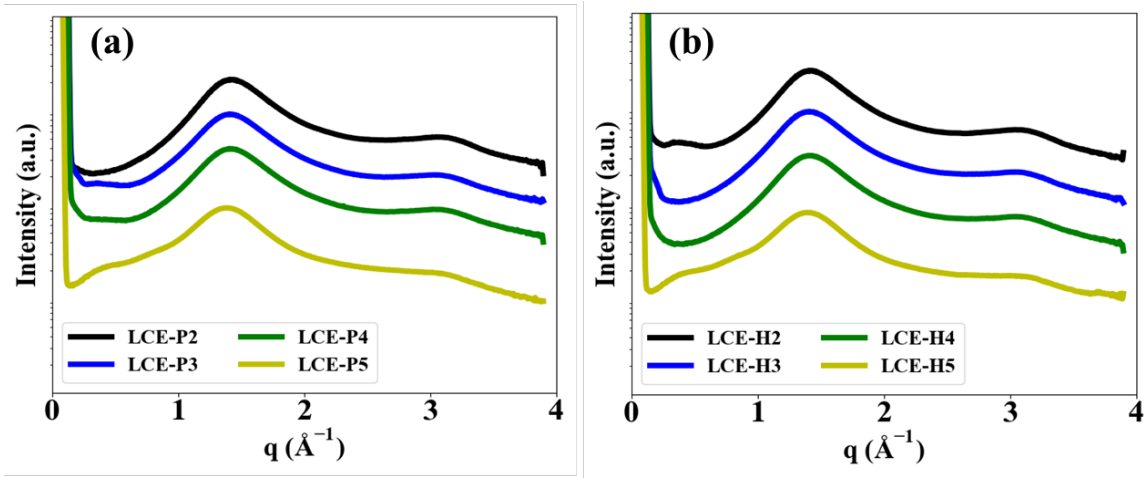

Figure S2: 1D Wide Angle X-ray (WAXS) profiles of LCE-Xn (n=2-5) before use them in batteries. Exposure time is 5 minutes for all samples. (a) Planar, and (d) Homeotropic electrolytes.

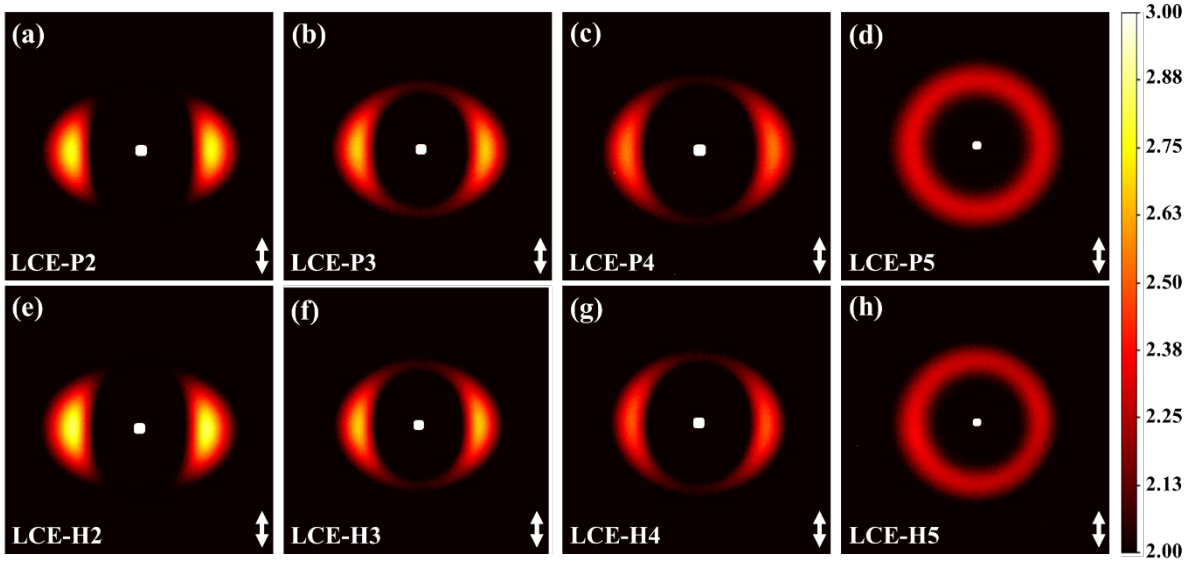

Figure S3: 2D Wide Angle X-ray (WAXS) profiles of LCE-Xn (n=2-5) before use in batteries. White double-sided arrows indicate the original alignment directions. Exposure time is 5 minutes for all samples. a) LCE-P2, (b) LCE-P3, (c) LCE-P4, (d) LCE-P5, (e) LCE-H2, (f) LCE-H3, (g) LCE-H4, and (h) LCE-H5.

Polarized Optical Microscopy (POM) studies of the elastomers are presented in **Figures S4–S8**. For the LCE-X1 samples, both planar and homeotropic cells exhibited partial alignment prior to stretch-induced polymerization. After polymerization, both configurations demonstrated significant improvement in alignment, as evidenced by the characteristic black textures parallel or perpendicular to the polarizers and bright textures at 45° relative to the polarizers as shown in **Figure S4**. The homeotropic cells displayed a few minor "+" defects, likely corresponding to localized disclinations, but overall, the texture remained uniform and continuous, indicating effective long-range molecular ordering. These observations highlight the initial influence of mechanical pre-alignment on the final molecular orientation of the elastomer network.

For the LCE-X2 samples, planar cells initially displayed only partial alignment, whereas the homeotropic cells appeared well-aligned even before stretching, suggesting that the homeotropic configuration inherently favors more ordered molecular packing under the same preparation conditions. Following stretch-induced polymerization, both planar and homeotropic cells showed a pronounced enhancement in alignment, with brighter birefringent patterns and sharper contrast under crossed polarizers, shown in **Figure S5**. This trend continued for the LCE-X3 samples like shown in **Figure S6**, where both configurations exhibited further improvement in alignment quality. By the time the LCE-X4 samples were examined, the elastomers were already well-aligned prior to polymerization, and subsequent stretching and curing only enhanced the ordering. Across all compositions, the homeotropic configuration consistently exhibited the highest optical extinction, indicating the most efficient alignment of mesogens and corroborating the directional control imparted by the initial cell orientation as shown in **Figure S7**.

In contrast, the LCE-X5 samples demonstrated no visible alignment when 2 wt.% dipropylamine (DPA) was used as the catalyst, indicating that excessive cross-linking may impede the ability of the mesogens to organize. However, reducing the DPA concentration to 0.5 wt.% led to the emergence of clear alignment, highlighting the critical role of catalyst concentration in controlling the balance between cross-linking density and molecular mobility as shown in **Figure S8**. This behavior is further influenced by the presence of BMIM-TFSI in the system. While BMIM-TFSI is not strongly basic, it shares the same cation as BMIM-OH, a basic ionic liquid known to catalyze Michael additions, including thiol additions to α,β-acetylenic ketones and additions of active methylene compounds to conjugated ketones and nitriles.[3] These observations support the hypothesis that DPA, particularly when acting in synergy with BMIM-TFSI, can enhance the reaction kinetics, potentially leading to excessive cross-linking at higher concentrations. By carefully optimizing the catalyst content, sufficient molecular mobility is retained, allowing the elastomer network to achieve optimal mesogen alignment, as clearly evidenced in the reduced DPA samples.

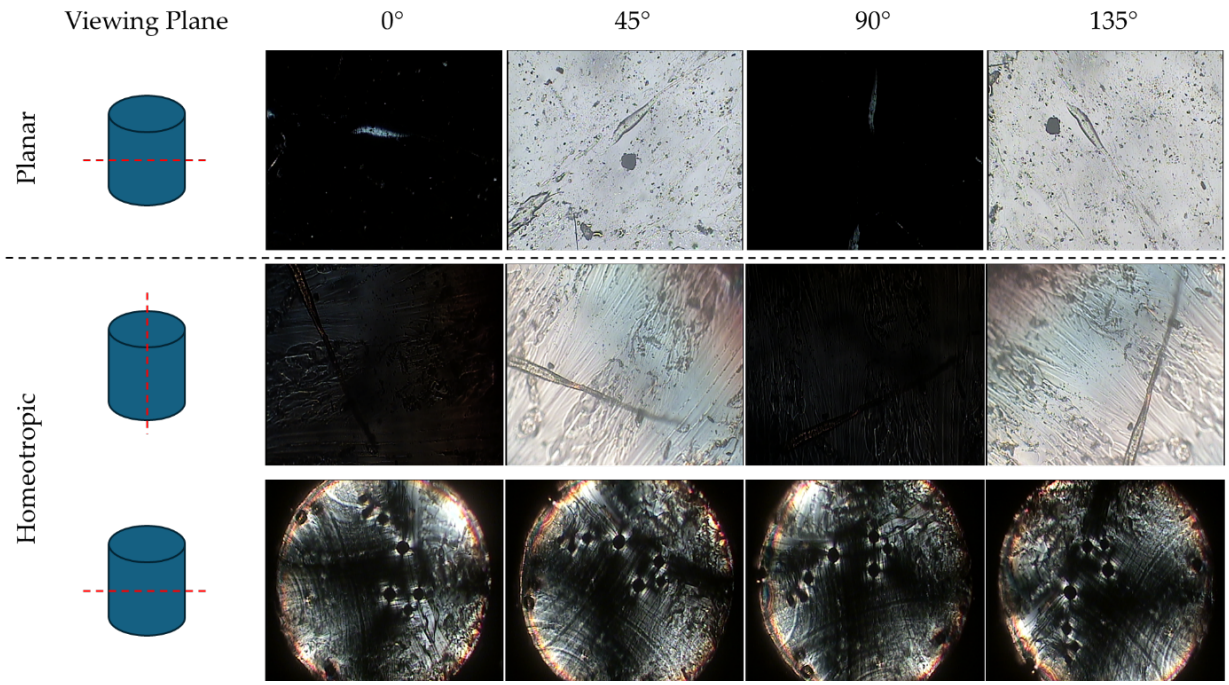

Figure S4: POM textures of LCE-X1 electrolytes with 5 mg of IL loading - observed under crossed polarizers at relative rotation angles of 0°, 45°, 90°, and 135°, captured from various focal planes, including side and top views:

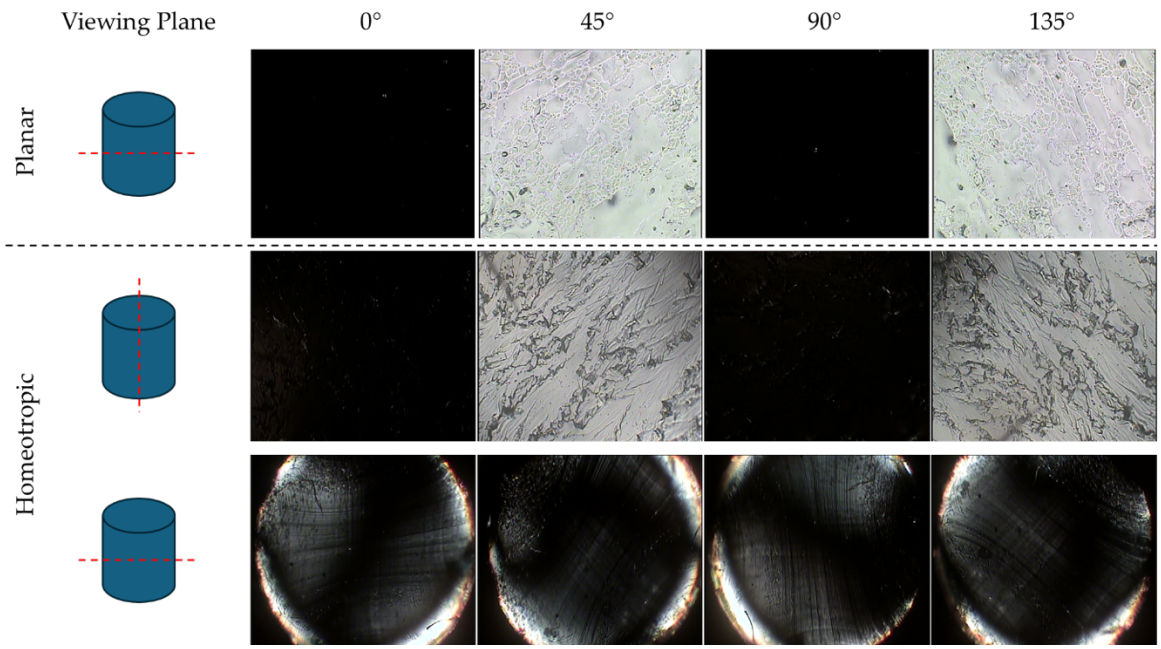

Figure S5: POM textures of LCE-X2 electrolytes with 250 mg of IL loading - observed under crossed polarizers at relative rotation angles of 0°, 45°, 90°, and 135°, captured from various focal planes, including side and top views.

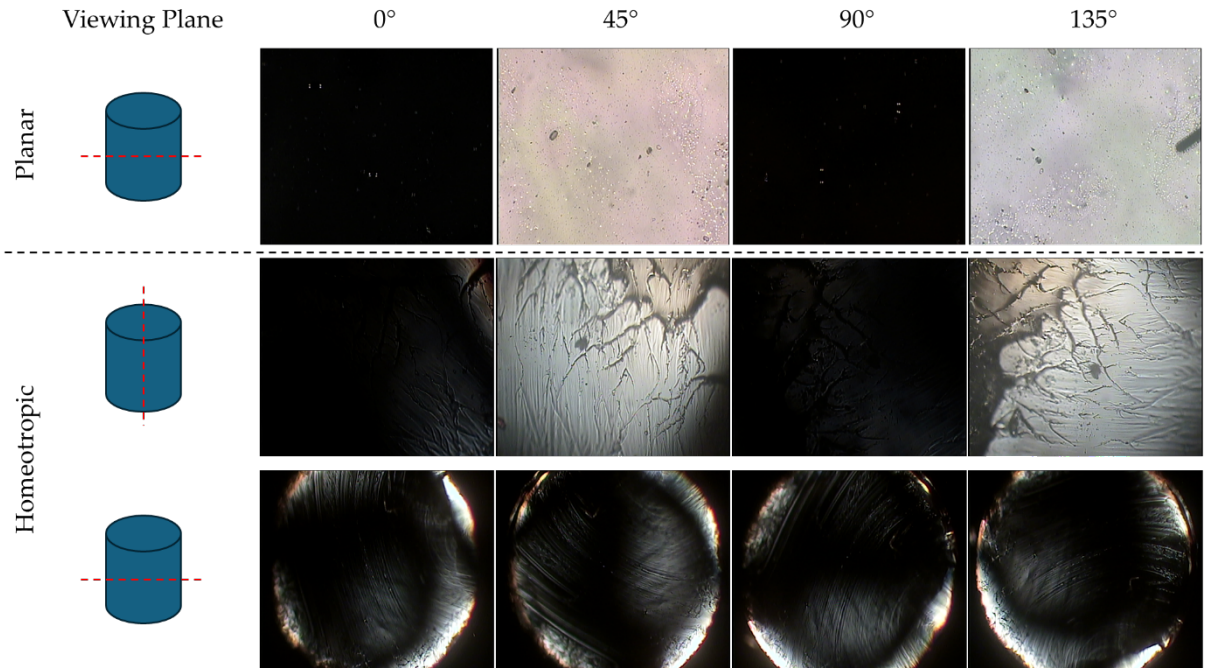

Figure S6: POM textures of LCE-X3 electrolytes with 500 mg of IL loading - observed under crossed polarizers at relative rotation angles of 0°, 45°, 90°, and 135°, captured from various focal planes, including side and top views.

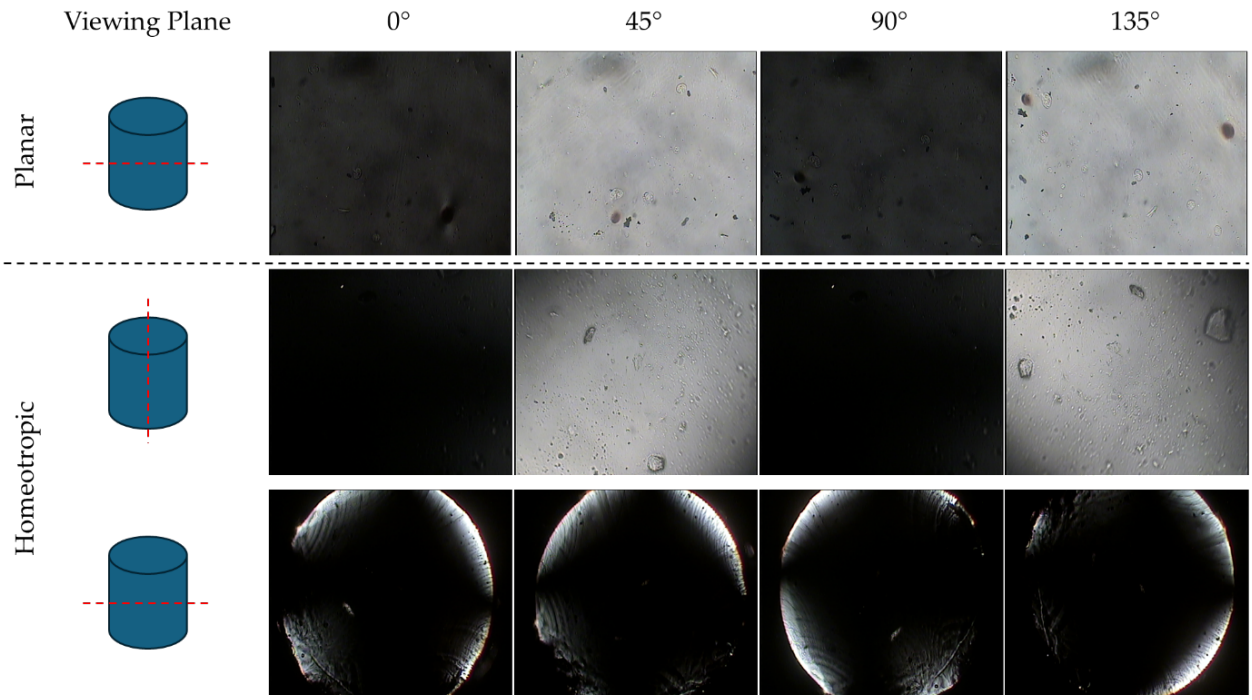

Figure S7: POM textures of LCE-X4 electrolytes with 1.00 g of IL loading - observed under crossed polarizers at relative rotation angles of 0°, 45°, 90°, and 135°, captured from various focal planes, including side and top views.

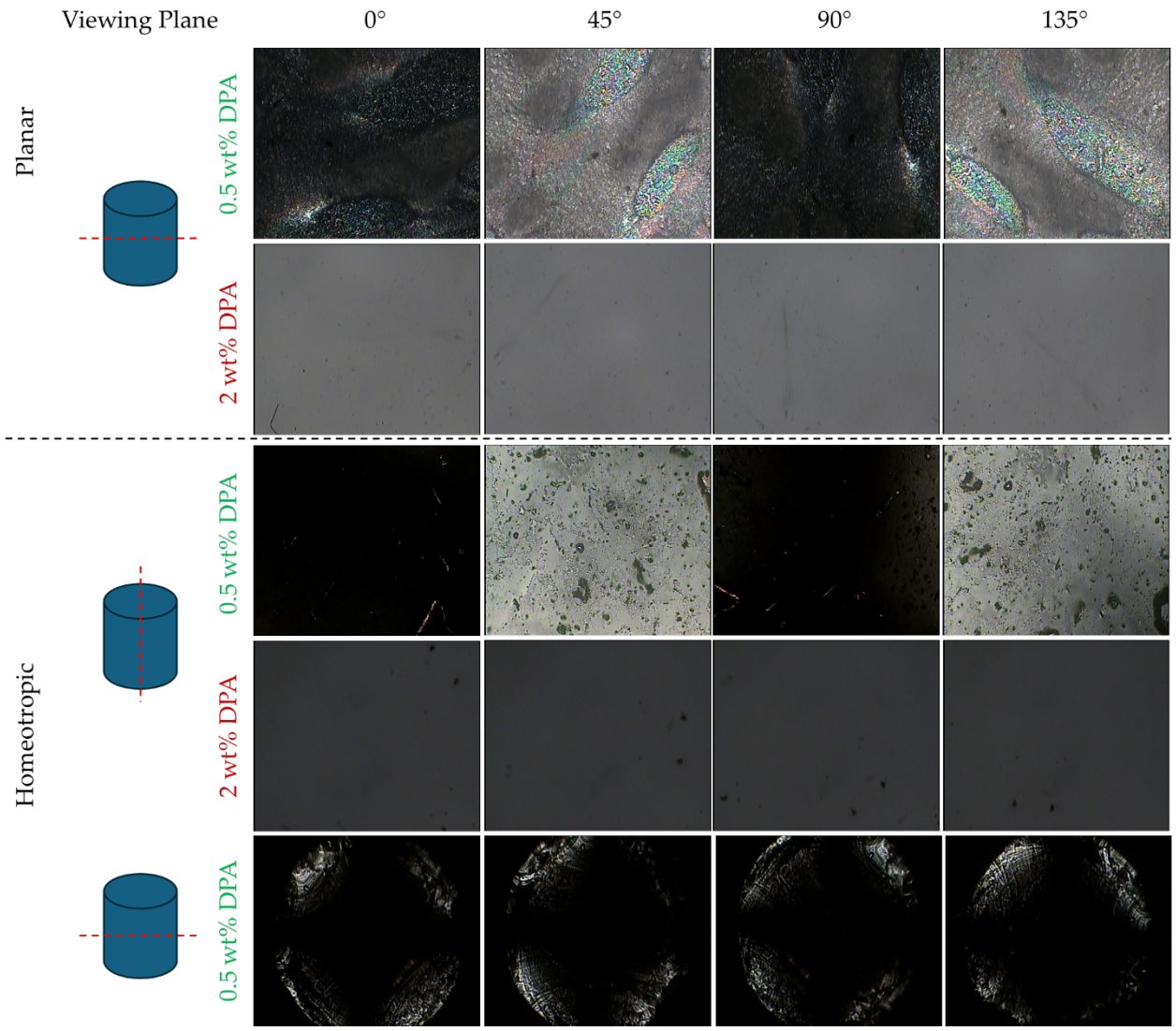

Figure S8: POM textures of LCE-X5 electrolytes with 1.50 g of IL loading - observed under crossed polarizers at relative rotation angles of 0°, 45°, 90°, and 135°, captured from various focal planes, including side and top views.

All samples were examined by Field Emission-Scanning Electron Microscopy (FE-SEM) imaging without prior drying, allowing the ionic liquid to remain visible as it oozes out of the ion channels within the elastomer matrix. Surface images were captured using a flat stage, while cross-sectional images were obtained using a 45° tilt stage at the central region of the bulk, equidistant from both surfaces. To expose the cross-section, the elastomer was manually torn perpendicular to the director instead of cutting with a blade. We note that the rough edges of the blade can leave unwanted surface artifacts and compress the elastomer at the cutting site. This compression can distort or collapse the ion channels or pores, making them less visible in imaging. FE-SEM revealed distinct morphological changes as the IL content increased (see **Figure S9**).[4]

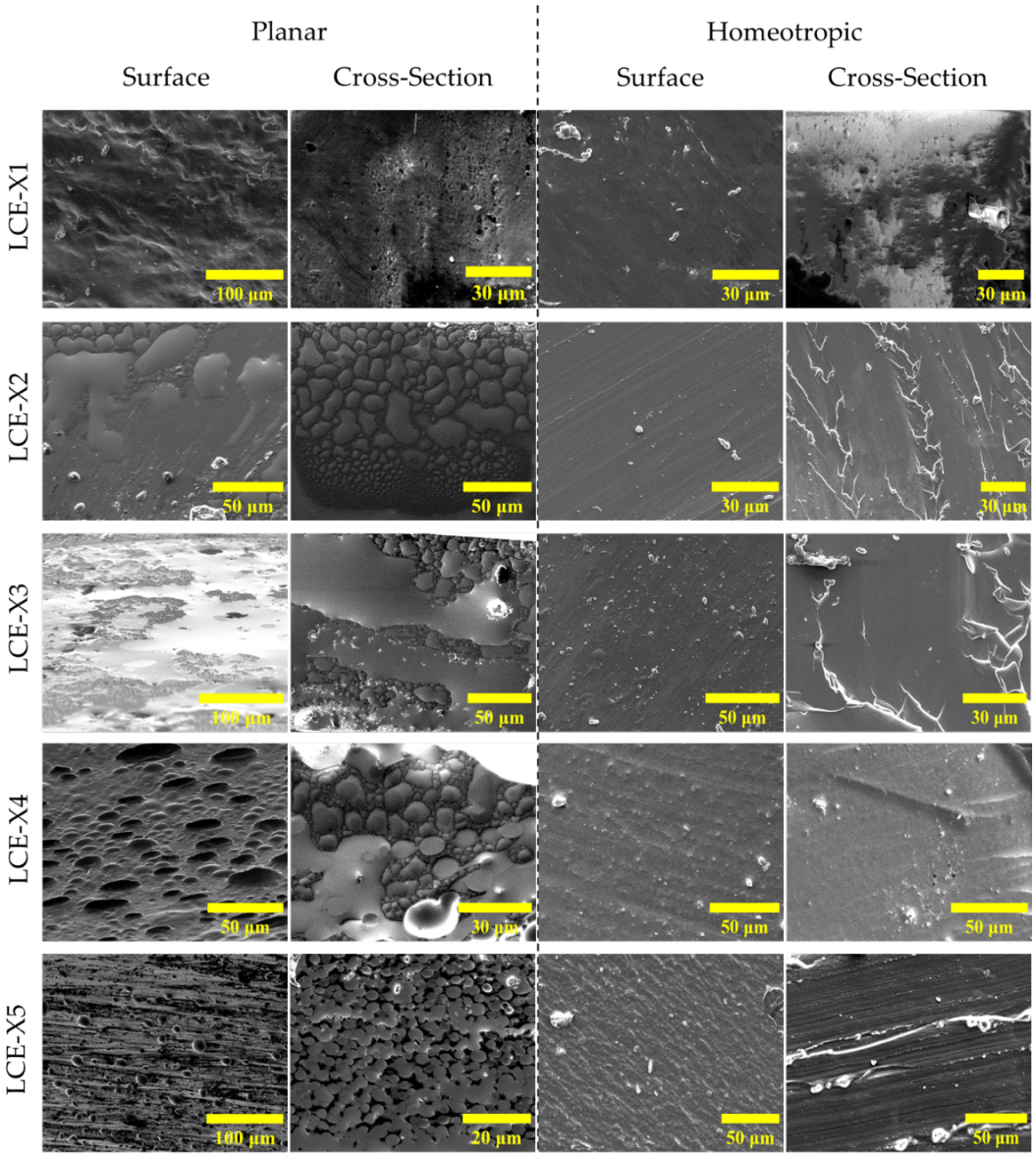

Figure S9: FE-SEM images of planar (left) and homeotropic (right) electrolyte samples, showing vertical and horizontal cross-sections. From top to bottom, the ionic liquid (IL) concentration increases from 0.67% to 66.67%, corresponding to LCE-Xn (n = 1, 2, 3, 4, 5).

In 100 µm thick planar samples, clear evidence of IL expulsion through surface and internal pores was observed, with pore density increasing consistently with IL concentration. This trend suggests that higher IL loadings disrupt the uniformity of the polymer network, creating more channels and voids. In 100 µm thick homeotropic samples, except for the LCE-H3 sample, pores were mostly absent. This could be due to the greater thickness of these films preventing IL from escaping under high vacuum conditions of SEM, unlike the earlier drying step during sample preparation which used a gentler vacuum. Most homeotropic cross-sections appeared smooth, featuring linear striations likely caused by the microtome's diamond blade during sectioning. In contrast, planar cross-sections did not have these lines indicating tearing rather than clean cutting but showed more visible porosity throughout. Note for the samples LCE-X4 and LCE-X5 samples surface-level pores were also observed, indicating a correlation between IL concentration and pore formation within the polymer matrix.

Electrochemical Impedance Spectroscopy (EIS) measurement results of planar samples LCE-Pn (n = 2, 3, 4, 5) are shown in **Figure S10** and the values of measured ionic conductivities are listed in **Table S2**.

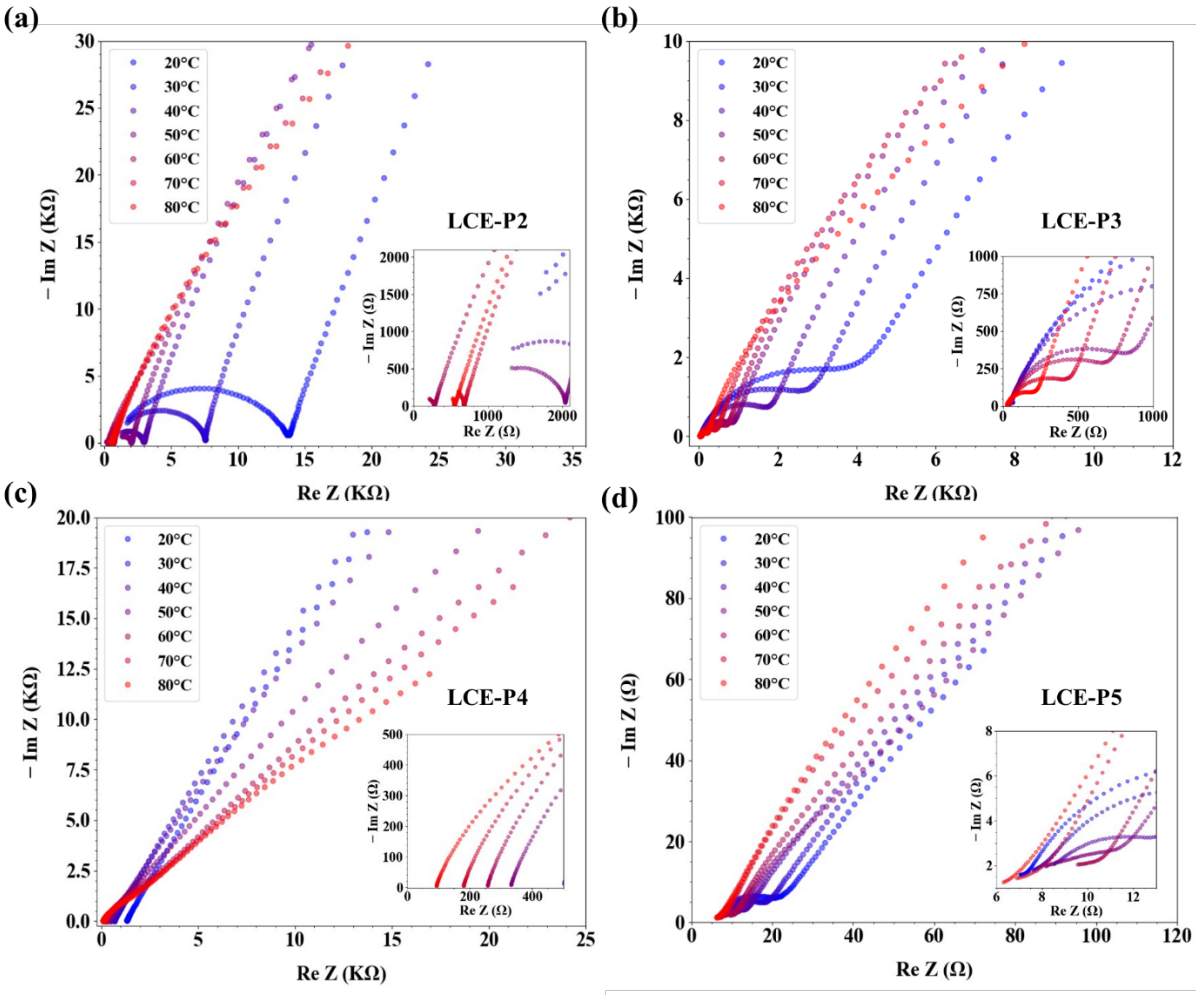

Figure S10: Nyquist plots of electrochemical impedance spectroscopy of planar-aligned electrolytes measured from 20 °C to 80 °C in 10 °C increments over a frequency range of 1 Hz to 1 MHz.

Table S2: Average electrochemical impedance spectroscopy (EIS) conductivity vs. temperature for planar electrolytes with increasing ionic liquid (IL) content.

		20 °C	30 °C	40 °C	50 °C	60 °C	70 °C	80 °C
Ionic Conductivity S · cm^{-1}	LCE-P1	1.37×10^{-7}	3.33×10^{-7}	6.11×10^{-7}	1.73×10^{-6}	3.24×10^{-6}	5.83×10^{-6}	8.24×10^{-6}
	LCE-P2	1.02×10^{-6}	1.86×10^{-6}	4.71×10^{-6}	6.91×10^{-6}	1.18×10^{-5}	2.04×10^{-5}	2.56×10^{-5}
	LCE-P3	3.36×10^{-6}	5.65×10^{-6}	9.64×10^{-6}	1.80×10^{-5}	2.35×10^{-5}	3.69×10^{-5}	6.00×10^{-5}
	LCE-P4	1.06×10^{-5}	2.10×10^{-5}	2.79×10^{-5}	4.21×10^{-5}	5.44×10^{-5}	7.76×10^{-5}	1.50×10^{-4}
	LCE-P5	7.75×10^{-4}	9.22×10^{-4}	1.24×10^{-3}	1.35×10^{-3}	1.61×10^{-3}	1.90×10^{-3}	2.22×10^{-3}

EIS measurement of homeotropic samples LCE-Hn (n = 2, 3, 4, 5) are shown in **Figure S11** and the values of measured ionic conductivities are listed in **Table S3**.

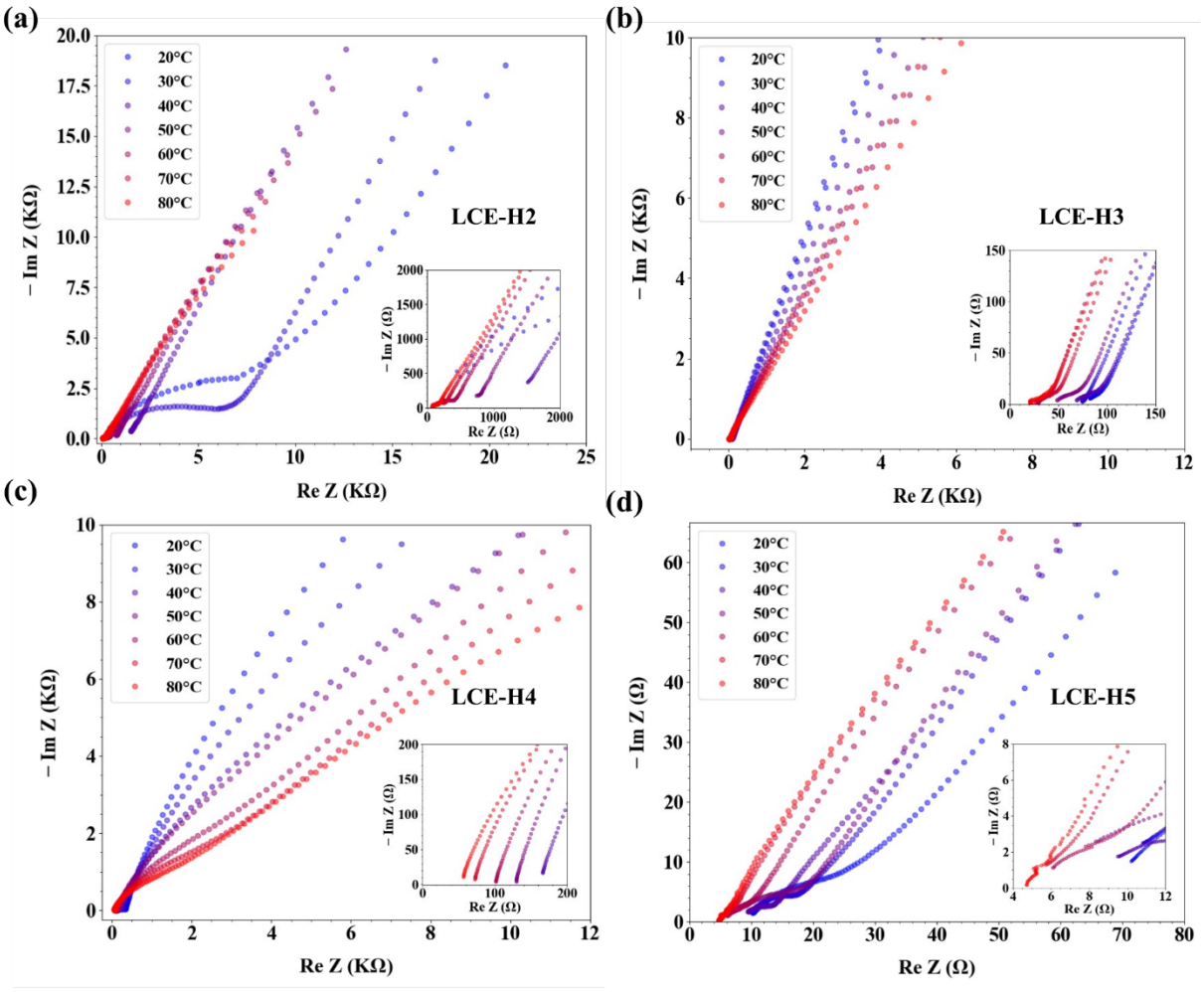

Figure S11: Electrochemical impedance spectroscopy of homeotropic-aligned electrolytes measured from 20 °C to 80 °C in 10 °C increments over a frequency range of 1 Hz to 1 MHz

Table S3: Average electrochemical impedance spectroscopy (EIS) conductivity vs. temperature for homeotropic electrolytes with increasing ionic liquid (IL) content.

		20 °C	30 °C	40 °C	50 °C	60 °C	70 °C	80 °C
Ionic Conductivity S · cm^{-1}	LCE-H1	7.40×10^{-8}	1.69×10^{-7}	3.64×10^{-7}	7.51×10^{-6}	1.48×10^{-6}	2.81×10^{-6}	5.14×10^{-6}
	LCE-H2	1.14×10^{-6}	1.53×10^{-6}	3.04×10^{-6}	7.98×10^{-6}	9.30×10^{-6}	1.22×10^{-5}	1.70×10^{-5}
	LCE-H3	8.07×10^{-6}	1.29×10^{-5}	2.19×10^{-5}	3.00×10^{-5}	4.25×10^{-5}	6.74×10^{-5}	9.22×10^{-5}
	LCE-H4	4.21×10^{-5}	5.49×10^{-5}	8.42×10^{-5}	1.08×10^{-4}	1.38×10^{-4}	1.94×10^{-4}	2.50×10^{-4}
	LCE-H5	1.22×10^{-3}	1.40×10^{-3}	1.76×10^{-3}	1.83×10^{-3}	2.13×10^{-3}	2.47×10^{-3}	2.63×10^{-3}

To calculate the average overpotential, the cyclic voltammetry (CV) data were analyzed. The overpotential (η) is defined as the difference between the anodic (E_{pa}) or cathodic (E_{pc}) peak potentials with respect to the Open Circuit Potential (OCV):

$$\eta = \left|\mathrm{E_{pa}} - \mathrm{E_{OCV}}\right| = \left|\mathrm{E_{pc}} - \mathrm{E_{OCV}}\right|$$

The OCV for each sample was approximated as the average of the anodic and cathodic peak potentials, i.e.,

$$\mathrm{E_{OCV}} = \frac{\mathrm{E_{pa}} + \mathrm{E_{pc}}}{2}$$

The peak potential values extracted from the CV curves are summarized below:

Table S4: Extracted anodic ($\mathbf{E_{pa}}$) and cathodic ($\mathbf{E_{pc}}$) peak potentials corresponding open-circuit potentials ($\mathbf{E_{OCV}}$), and calculated overpotentials (η) for the LCE-based solid polymer electrolyte samples obtained from cyclic voltammetry measurements.

Sample	$\mathbf{E_{pa}}$ (V)	$\mathbf{E_{pc}}$ (V)	$\mathbf{E_{OCV}}$ (V)	η (V)
LCE-P4	4.2 ± 0.1	3.1 ± 0.1	3.65 ± 0.1	0.6 ± 0.1
LCE-H4	4.0 ± 0.2	3.3 ± 0.1	3.65 ± 0.2	0.4 ± 0.2
LCE-P5	4.2 ± 0.2	3.1 ± 0.1	3.65 ± 0.2	0.6 ± 0.2
LCE-H5	4.2 ± 0.2	2.9 ± 0.1	3.55 ± 0.2	0.7 ± 0.2

Thus, the average overpotential across the four samples is:

$$\bar{\eta} = \frac{0.6 + 0.4 + 0.6 + 0.7}{4} \approx 0.54\ V$$

The calculated average overpotential of approximately 0.54 ± 0.20 V is typical for solid polymer electrolyte systems, where limited ionic mobility and interfacial resistance contribute to higher polarization compared to liquid electrolytes. However, among the samples, LCE-H4 shows slightly lower overpotential, indicating more favorable redox reversibility, possibly due to enhanced ion transport or better structural alignment within the liquid crystal elastomer matrix.

EIS measurements of symmetric Li/LCE-Xn/Li (n = 2-5) cells, shown for planar (**Figure S12(a)**) and homeotropic (**Figure S12(b)**) alignments, were used to determine the Li-ion transference number (**Figure S12(d)**). Nyquist plots were recorded before polarization to find the initial interfacial resistance (R_0) and after polarization with a 10 mV DC bias to find the steady-state resistance (R_s). Frequencies below 1 kHz were excluded from the EIS data due to high noise. The corresponding chronoamperometry fall-current profile, shown in **Figure S12(c)** for both alignments, was used to determine the initial (I_0) and steady-state (I_S) currents.

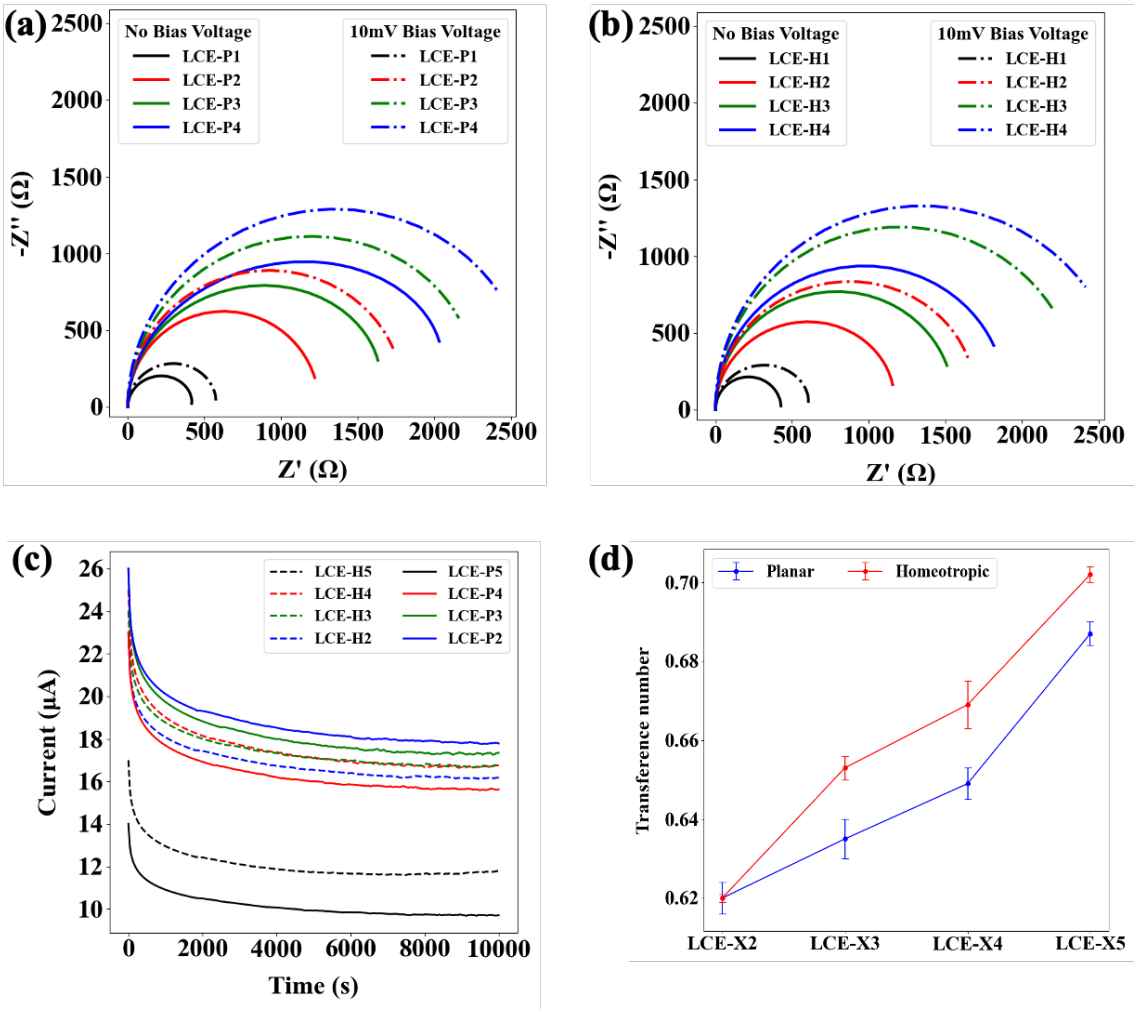

Figure S12: Electrochemical impedance spectroscopy of Li/LCE-Xn/Li symmetric cells before and after polarization at 10 mV from 1 kHz to 1MHz. (a) Planar and (b) homeotropic electrolytes; (c) corresponding current decay curves during polarization and (d) calculated transference numbers.

The figures clearly show that the semicircles measured after applying the 10 mV bias (representing R_s) have a much larger radius than the initial ones (representing R_0). This indicates a significant increase in interfacial resistance. This phenomenon is caused by cell polarization: the applied 10 mV bias forces the Li^+ ions and the counter-anions to move at different speeds. Because the ions are not moving at the same rate, a concentration gradient builds up within the electrolyte, which in turn creates an internal field that opposes the applied voltage. This gradient is responsible for the new, higher resistance (R_s) measured in the final EIS scan, and the large difference between R_0 and R_s confirms this gradient has formed.

The chronoamperometry profile in **Figure S12(c)** visualizes this polarization process over time. The initial current (I_0) is the peak value measured the instant the 10 mV bias is applied, representing the total ionic conductivity before a significant concentration gradient forms. As this gradient builds up, it increasingly opposes the ion flow, causing the current to "fall" or decay until it reaches a stable steady-state current (I_S).

Cycled electrolytes (LCE-P5 and LCE-H4) were extracted from CR2032 coin cells in an Ar-gas filled glovebox. To flush the ionic liquid, the electrolytes were submerged in methanol under vacuum at room temperature for 24 hours, washed with fresh methanol, and subsequently dried in a vacuum oven at 90°C for another 24 hours. The samples were cooled to room temperature before imaging. It was noted that the LFP cathode remained firmly attached to the electrolyte surface even after this process; therefore, high light intensity was required for the POM to penetrate the sample.

The resulting POM textures are shown in Figure S13. The planar LCE-P5 sample displays a bright texture when rotated 45° relative to the crossed polarizers, indicating that its alignment was retained post-cycling. The homeotropic LCE-H4 sample remains mostly dark at all rotation angles. While this observation is consistent with homeotropic alignment, it is less conclusive.

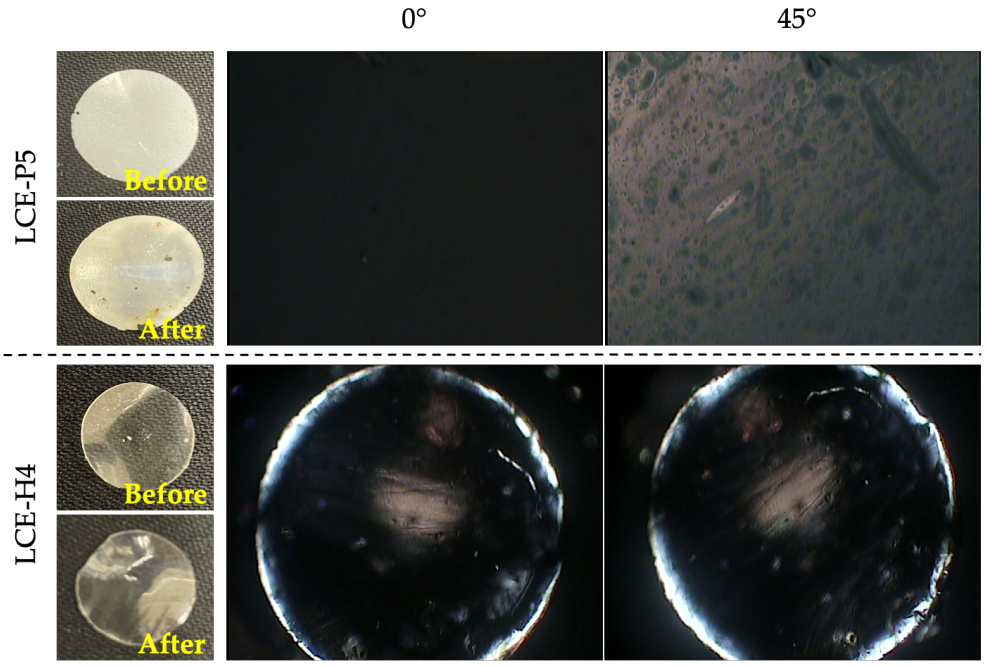

Figure S13: Crossed polarized optical microscopy images of LCE-P5 (top) LCE-H4 (bottom) electrolytes after 300 charge–discharge cycles, taken at rotation angles of 0°, 45°.

The 1D WAXS intensity vs. q data for post-cycle analysis is presented in **Figure S14**. The spectra for LCE-X3 and LCE-X4 show no discernable change, remaining consistent with their pre-cycle spectra (**Figure S2**). However, a notable change is observed in LCE-X5, which exhibits a new, second peak at $q{\sim}0.8\text{Å}^{-1}$. We attribute the appearance of this peak to the phase separation of the ionic liquid (IL) post-cycling, which is likely a result of the high 66.7 wt.% IL concentration in this sample.

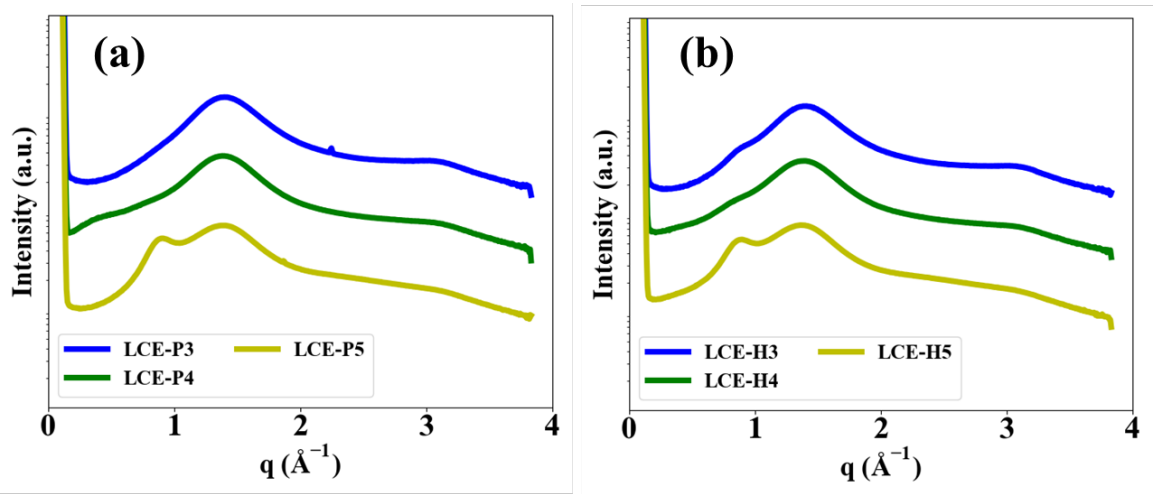

Figure S14: 1D Wide Angle X-ray (WAXS) profiles of LCE-Xn (n = 3-5) post-cycle in Li-ion batteries. Exposure time is 5 minutes for all samples. (a) Planar, and (d) Homeotropic electrolytes.

References

1 M. O. Saed, A. H. Torbati, D. P. Nair and C. M. Yakacki, *Journal of Visualized Experiments*, 2016, **2016**, e53546.

2 J. Anthony Dicks and C. Woolard, *Macromol Mater Eng*, 2025, **310**, 2400445.

3 B. C. Ranu, S. Banerjee and R. Jana, *Tetrahedron*, 2007, **63**, 776–782.

4 P. H. Hermans and P. Platzek, *Kolloid-Zeitschrift*, 1939, **88**, 68–72.